Some issues concerning Large-Eddy Simulation of inertial particle dispersion in turbulent bounded flows

C. Marchioli[1], M.V. Salvetti[2] and A. Soldati[1,*] *

[1] *Dept. Energy Technology and Centro Interdipartimentale di Fluidodinamica e Idraulica, University of Udine, 33100 Udine – Italy*

[2] *Dept. Aerospace Engineering, University of Pisa, 56100 Pisa – Italy*

ABSTRACT

The problem of an accurate Eulerian-Lagrangian modeling of inertial particle dispersion in Large Eddy Simulation (LES) of turbulent wall-bounded flows is addressed. We run Direct Numerical Simulation (DNS) for turbulent channel flow at $Re_\tau = 150$ and 300 and corresponding *a priori* and *a posteriori* LES on differently coarse grids. We then tracked swarms of different inertia particles and we examined the influence of filtering and of Sub-Grid Scale (SGS) modeling for the fluid phase on particle velocity and concentration statistics. We also focused on how particle preferential segregation is predicted by LES. Results show that even "well-resolved" LES is unable to reproduce the physics as demonstrated by DNS, both for particle accumulation at the wall and for particle preferential segregation. Inaccurate prediction is observed for the entire range of particles considered in this study, even when the particle response time is much larger than the flow timescales not resolved in LES. Both *a priori* and *a posteriori* tests indicate that recovering the level of fluid and particle velocity fluctuations is not enough to have accurate prediction of near-wall accumulation and local segregation. This may suggest that reintroducing the correct amount of higher-order moments of the velocity fluctuations is also a key point for SGS closure models for the particle

**Author to whom correspondence should be addressed. Also affiliated with Department of Fluid Mechanics, CISM, 33100 Udine, Italy. Electronic Mail: soldati@uniud.it.

equation. Another important issue is the presence of possible flow Reynolds number effects on particle dispersion. Our results show that, in small Reynolds number turbulence and in the case of heavy particles, the shear fluid velocity is a suitable scaling parameter to quantify these effects.

1. INTRODUCTION

The dispersion of inertial particles in turbulent flows is characterized by macroscopic phenomena such as non-homogeneous distribution, large-scale clustering and preferential concentration due to the inertial bias between the denser particles and the lighter surrounding fluid.[1,2] In homogeneous isotropic turbulence,[1,3,4] clustering and preferential concentration may be crucial in determining collision frequency, breakage efficiency, agglomeration and reaction rates. Focusing on turbulent boundary layer, we observe that, besides controlling particle interaction rates, these phenomena strongly influence settling, deposition and entrainment.[5]

Both Direct Numerical Simulation (DNS)[2,6] and Large-Eddy Simulation (LES)[7–9] together with Lagrangian Particle Tracking (LPT) have been widely used to investigate and quantify these macroscopic phenomena, for instance in channel[2,8,9] or in pipe flows.[6,7] DNS-based Eulerian-Lagrangian studies are widely used for investigating the physics of particle-turbulence interactions, whereas LES has yet to demonstrate its full capabilities in predicting correctly particle-turbulence statistics[10] and macroscopic segregation phenomena.[4,9] In previous studies on particle dispersion in turbulent bounded flows,[10,9] LES methods were found inadequate to predict local segregation phenomena which eventually control macroscopic fluxes. This inadequacy was attributed to the filtering of the flow Sub-Grid Scales (SGS). To elaborate, in LES-based Eulerian-Lagrangian simulations of particle dispersion a *sub-grid* error is introduced in the particle equation since only the filtered fluid velocity is available; this approximation adds to the *modeling* error which is intrinsic to the SGS modeling.[10] Similar to what is done for the flow field, a way to model the effects of the filtered SGS velocity fluctuations on particle motion should be identified.[9]

Among previous LES applications to gas-solid turbulent flows,[7,11] the SGS velocity fluctuations were neglected based on the assumption that the particle response time was large compared to the smallest timescale resolved in the LES.[11] It was later demonstrated that this assumption leads to a certain degree of inaccuracy on the prediction of particle velocity statistics and concentration. In particular, the results obtained by Kuerten and Vreman[10] and by Kuerten[9] for turbulent dispersion of heavy particles in channel flow have shown that, due to both sub-grid and modeling errors, LES underestimates the tendency of particles to move towards the wall by the effect of the turbulence (turbophoretic effect[12]). To circumvent this problem, a closure model for the particle equation of motion based on filter inversion by approximate deconvolution was proposed to recover the influence of the filtered scales in turbulent channel flow[9] and in homogeneous turbulent shear flow.[13]

An effort was also provided to establish criteria according to which the SGS modeling for particles could be judged necessary or not. In particular, Février *et al.*[14] have shown that LES filtering has an effect on particle motion which depends on the ratio of the particle size to the filtered spatial scales. Fede and Simonin[4] have studied the influence of sub-grid fluid velocity fluctuations on particle dispersion, preferential concentration, and inter-particle collisions in homogeneous isotropic turbulence. For single particle statistics such as turbulent dispersion, Fede and Simonin[4] confirm that an explicit accounting of sub-grid fluid turbulence on particle transport is not required when the particle response time is much larger than the cut-off timescale of the sub-grid velocities. However, they show also that accumulation and collision phenomena are strongly influenced by sub-grid fluid turbulence even when the particle response time is up to $\mathcal{O}(10)$ times the Kolmogorov time scale.

Aim of the present study is precisely to build on the work of Kuerten and Vreman[10] extending the analysis of Fede and Simonin[4] on the sub-grid turbulence effects on particle accumulation (neglecting inter-particle collisions) to turbulent channel flow, which presents the additional complexity of a solid wall and of turbulence strong anisotropy and non-homogeneity. The analysis is grounded on a systematic investigation on the importance of SGS effects on particle motion for different particle inertia and under different flow conditions. The specific objectives of the present study can be summarized as follows: *(i)*

Create a database for particle-laden turbulent channel flow in which different values of the flow Reynolds number and of the particle response time are considered, showing in this paper particle velocity and concentration statistics reported from DNS/LES computed at shear Reynolds number up to 300 and grid resolution up to 256^3 grid points. *(ii)* Use this database to investigate on the importance of the SGS velocity fluctuations in predicting the statistical properties of the dispersion process. We will focus on the effects due to changes in particle inertia (obtained by tuning of the particle size with respect to the filtered spatial scales) or in grid resolution as well as on possible flow Reynolds number scaling properties of particle preferential concentration. *(iii)* Provide subsidies for the development of new SGS closure models for the equations of particle motion.

The paper is organized as follows. Problem statement, governing equations and numerical methodology required for the simulations are presented in Sec. 2. Sec. 3 is devoted to the analysis and discussion of relevant statistics obtained from simulations where particle trajectiores are computed from DNS, filtered DNS in *a priori* tests and LES in *a posteriori* tests. In this case the discussion will be focused on the quantification of sub-grid and modeling errors on particle velocity and concentration statistics as well as on particle preferential distribution, thus extending the analysis of Kuerten and Vreman.[10] Finally, conclusions and future developments are drawn in Sec. 4.

2. PHYSICAL PROBLEM AND NUMERICAL METHODOLOGY

2.1. Particle-laden turbulent channel flow

The flow into which particles are introduced is a turbulent channel flow of gas. In the present study, we consider air (assumed to be incompressible and Newtonian) with density $\rho = 1.3\ kg\ m^{-3}$ and kinematic viscosity $\nu = 15.7{\times}10^{-6}\ m^2\ s^{-1}$. The governing balance equations for the fluid (in dimensionless form) read as:

$$\frac{\partial u_i}{\partial x_i} = 0 \ , \tag{1}$$

$$\frac{\partial u_i}{\partial t} = -u_j \frac{\partial u_i}{\partial x_j} + \frac{1}{Re} \frac{\partial^2 u_i}{\partial {x_j}^2} - \frac{\partial p}{\partial x_i} + \delta_{1,i} \ , \tag{2}$$

where u_i is the i^{th} component of the dimensionless velocity vector, p is the fluctuating kinematic pressure, $\delta_{1,i}$ is the mean dimensionless pressure gradient that drives the flow and $Re_\tau = u_\tau h/\nu$ is the shear Reynolds number based on the shear (or friction) velocity, u_τ, and on the half channel height, h. The shear velocity is defined as $u_\tau = (\tau_w/\rho)^{1/2}$, where τ_w is the mean shear stress at the wall. All variables considered in this study are reported in dimensionless form, represented by the superscript + (which has been dropped from Eqns. (1) and (2) for ease of reading) and expressed in wall units. Wall units are obtained combining u_τ, ν and ρ.

In LES, the standard Continuity and Navier-Stokes equations are smoothed with a filter function of width Δ. Accordingly, all flow variables are decomposed into a resolved (large-scale) part and a residual (sub-grid scale) part as $\mathbf{u}(\mathbf{x},t) = \bar{\mathbf{u}}(\mathbf{x},t) + \delta\mathbf{u}(\mathbf{x},t)$. The filtered Continuity and Navier-Stokes equations for the resolved scales are then:

$$\frac{\partial \bar{u}_i}{\partial x_j} = 0 \ , \tag{3}$$

$$\frac{\partial \bar{u}_i}{\partial t} = -\bar{u}_j \frac{\partial \bar{u}_i}{\partial x_j} + \frac{1}{Re}\frac{\partial^2 \bar{u}_i}{\partial {x_j}^2} - \frac{\partial \bar{p}}{\partial x_i} + \delta_{1,i} - \frac{\partial \tau_{ij}}{\partial x_j} \ , \tag{4}$$

where $\tau_{ij} = \overline{u_i u_j} - \bar{u}_i \bar{u}_j$ represents the sub-grid scale stress tensor. The large-eddy dynamics is closed once a model for τ_{ij} is provided. In the present study, the dynamic SGS model of Germano et al.[15] has been applied.

The reference geometry consists of two infinite flat parallel walls: the origin of the coordinate system is located at the center of the channel and the $x-$, $y-$ and $z-$ axes point in the streamwise, spanwise and wall-normal directions respectively (see Fig. 1). Periodic boundary conditions are imposed on the fluid velocity field in x and y, no-slip boundary conditions are imposed at the walls. The calculations were performed on a computational domain of size $4\pi h \times 2\pi h \times 2h$ in x, y and z respectively.

Particles with density $\rho_p = 1000\ kg\ m^{-3}$ are injected into the flow at concentration low enough to consider dilute system conditions. The motion of particles is described by a set of ordinary differential equations for particle velocity and position. For particles much heavier than the fluid ($\rho_p/\rho \gg 1$) Elghobashi and Truesdell[16] have shown that the most significant

forces are Stokes drag and buoyancy and that Basset force can be neglected being an order of magnitude smaller. In the present simulations, the aim is to minimize the number of degrees of freedom by keeping the simulation setting as simplified as possible; thus the effect of gravity has also been neglected. With the above assumptions, a simplified version of the Basset-Boussinesq-Oseen equation[17] is obtained. In vector form:

$$\frac{d\mathbf{x}}{dt} = \mathbf{v} \ , \tag{5}$$

$$\frac{d\mathbf{v}}{dt} = -\frac{3}{4}\frac{C_D}{d_p}\left(\frac{\rho}{\rho_p}\right)|\mathbf{v}-\mathbf{u}|(\mathbf{v}-\mathbf{u}) \ , \tag{6}$$

where $\mathbf{x}$ is particle position, $\mathbf{v}$ is particle velocity, and $\mathbf{u}$ is fluid velocity at particle position. The Stokes drag coefficient is computed as $C_D = \frac{24}{Re_p}(1+0.15Re_p^{0.687})$ where $Re_p = d_p|\mathbf{v}-\mathbf{u}|/\nu$ is the particle Reynolds number. The correction for C_D is necessary when Re_p does not remain small.

2.2. DNS and LES methodology

In this study both DNS and LES have been applied to the fully-developed channel flow. In both cases, the governing equations are discretized using a pseudo-spectral method based on transforming the field variables into wavenumber space, using Fourier representations for the periodic streamwise and spanwise directions and a Chebyshev representation for the wall-normal (non-homogeneous) direction. A two level, explicit Adams-Bashforth scheme for the non-linear terms, and an implicit Crank-Nicolson method for the viscous terms are employed for time advancement. Further details of the method have been published previously.[18]

DNS calculations have been performed using the parallel (MPI) version of the flow solver. Two values of the shear Reynolds number have been considered in this study: $Re_\tau = 150$ (Re_τ^l hereinafter) based on the shear velocity $u_\tau^l = 0.11775\ m\ s^{-1}$, and $Re_\tau = 300$ (Re_τ^h hereinafter) based on the shear velocity $u_\tau^h = 0.2355\ m\ s^{-1}$. The corresponding average (bulk) Reynolds numbers are $Re_b^l = u_b^l h/\nu = 1900$, where $u_b^l \simeq 1.49\ m\ s^{-1}$ is the average (bulk) velocity; and $Re_b^h = u_b^h h/\nu = 4200$, where $u_b^h \simeq 3.3\ m\ s^{-1}$, respectively. The size

of the computational domain in wall units is $1885 \times 942 \times 300$ for the Re_τ^l simulations and $3770 \times 1885 \times 600$ for the Re_τ^h simulations. The computational domain has been discretized in physical space with $128 \times 128 \times 129$ grid points (corresponding to 128×128 Fourier modes and to 129 Chebyshev coefficients in the wavenumber space) for the Re_τ^l simulations and with $256 \times 256 \times 257$ grid points (corresponding to 256×256 Fourier modes and to 257 Chebyshev coefficients in the wavenumber space) for the Re_τ^h simulations in order to keep the grid spacing fixed. This is the minimum number of grid points required in each direction to ensure that the grid spacing is always smaller than the smallest flow scale and that the limitations imposed by the point-particle approach are satisfied.[19]

LES calculations have been performed using the serial version of the pseudo-spectral flow solver on the same computational domain. Two computational grids have been considered: a *coarse* grid made of $32 \times 32 \times 65$ nodes and a *fine* grid made of $64 \times 64 \times 65$ nodes. Only the lower value, Re_τ^l, of the shear Reynolds number has been considered.

The complete set of DNS/LES simulations is summarized in Table I.

2.3. Filtering for *a priori* tests

In the *a priori* tests the Lagrangian tracking of particles is carried out starting from the filtered velocity field, $\bar{\mathbf{u}}$, obtained through explicit filtering of the DNS velocity by means of either a cut-off or a top-hat filter. Both filters are applied in the homogeneous streamwise and spanwise directions in the wave number space:

$$\bar{u}_i(\mathbf{x},t) = FT^{-1}\begin{cases} G(\kappa_1)\cdot G(\kappa_2)\cdot \hat{u}_i(\kappa_1,\kappa_2,z,t) & \text{if } |\kappa_j| \le |\kappa_c| \text{ with } j=1,2\ , \\ 0 & \text{otherwise}\ . \end{cases} \tag{7}$$

where FT is the 2D Fourier Transform, $\kappa_c = \pi/\Delta$ is the cutoff wave number (Δ being the filter width in the physical space), $\hat{u}_i(\kappa_1,\kappa_2,z,t)$ is the Fourier transform of the fluid velocity field, namely $\hat{u}_i(\kappa_1,\kappa_2,z,t) = FT[\bar{u}_i(\mathbf{x},t)]$ and $G(\kappa_i)$ is the filter transfer function:

$$G(\kappa_j) = \begin{cases} 1 & \text{for the cut-off filter}\ , \\ \frac{sin(\kappa_j\Delta/2)}{\kappa_j\Delta/2} & \text{for the top-hat filter}\ . \end{cases} \tag{8}$$

Three different filter widths have been considered at Re_τ^l, corresponding to a grid Coarsening Factor (CF in Table I) in each homogeneous direction of 2, 4 and 8 with respect to DNS. In the wall-normal direction data are not filtered, since often in LES the wall-normal resolution is DNS-like.[20]

2.4. Lagrangian particle tracking

To calculate particle trajectories in the flow field, we have coupled a Lagrangian tracking routine with the DNS/LES flow solver. The routine solves for Eqns. (6) and (5) using 6^{th}-order Lagrangian polynomials to interpolate fluid velocities at particle position; with this velocity the equations of particle motion are advanced in time using a 4^{th}-order Runge-Kutta scheme. The timestep size used for particle tracking was chosen to be equal to the timestep size used for the fluid, $\delta t^+ = 0.045$; the total tracking time was, for each particle set, $t^+ = 1200$ in the *a priori* tests and $t^+ = 1800$ in the *a posteriori* tests. These simulation times are not long enough to achieve a statistically steady state for the particle concentration.[21]

Particles, which are assumed pointwise, rigid and spherical, are injected into the flow at concentration low enough to neglect particle collisions. The effect of particles onto the turbulent field is also neglected (one-way coupling assumption). At the beginning of the simulation, particles are distributed homogeneously over the computational domain and their initial velocity is set equal to that of the fluid at the particle initial position. Periodic boundary conditions are imposed on particles moving outside the computational domain in the homogeneous directions, perfectly-elastic collisions at the smooth walls were assumed when the particle center was at a distance lower than one particle radius from the wall.

For the simulations presented here, large samples of 10^5 particles, characterized by different response times, were considered for each value of Re_τ. The response time is defined as $\tau_p = \rho_p d_p^2/18\mu$ where μ is the fluid dynamic viscosity: when the particle response time is made dimensionless using wall variables, the Stokes number for each particle set is obtained as $St = \tau_p^+ = \tau_p/\tau_f$ where $\tau_f = \nu/u_\tau^2$ is the viscous timescale of the flow. Tables II and III show all the parameters of the particles injected into the flow field. We remark here that, for

the present channel flow configuration at Re_τ^l, the non-dimensional value of the Kolmogorov timescale, τ_K^+, ranges from 2 wall units at the wall to 13 wall units at the channel centerline.[22] Hence, if we rescale the particle response times given in Table II using the local value of τ_K^+ near the centerline, where the flow conditions are closer to homogeneous and isotropic, we obtain Stokes numbers that vary from 10^{-2} to 10 and fall in the lower range of values considered by Fede and Simonin.[4]

As a further remark, we wish to add that the characteristic timescale of the flow changes depending on the specific value of the shear Reynolds number, namely on the specific value of the shear velocity. In the present case, we have $\tau_f^l = \nu / \left(u_\tau^l\right)^2 = 1.13 \cdot 10^{-3}\ s$ for the Re_τ^l simulations and $\tau_f^h = \nu / \left(u_\tau^h\right)^2 = 2.83 \cdot 10^{-4}\ s$ for the Re_τ^h simulations. Elaborating, we find that the same value of the Stokes number corresponds to different (dimensional) values of the particle response time according to the following expression:

$$St^l = St^h \rightarrow \frac{\tau_p^l}{\tau_f^l} = \frac{\tau_p^h}{\tau_f^h} \rightarrow \frac{\tau_p^l}{\tau_p^h} = \frac{\tau_f^l}{\tau_f^h} = \left(\frac{u_\tau^h}{u_\tau^l}\right)^2 = \left(\frac{Re_\tau^h}{Re_\tau^l}\right)^2 = 4\ , \tag{9}$$

where St^h and St^l represent the particle Stokes number in the Re_τ^l simulation and in the Re_τ^l simulation, respectively.

3. RESULTS

3.1. Particle distribution in *a priori* LES at Re_τ=150

In this Section, we will discuss the influence of filtering on particle distribution by showing the velocity statistics and the concentration profiles for particles dispersed in *a priori* LES flow fields, i.e. filtered DNS fields. We will also discuss filtering effects on local particle preferential segregation using macroscopic segregation parameters. As described in Sec. 2.3, the cut-off and the top-hat filters have been used; the first one provides a sharp separation between resolved and non-resolved scales and can be considered the filter corresponding to a coarse spectral simulation, in which no explicit filtering is applied. Conversely, the top-hat filter is a smooth filter and, thus, it subtracts a significant amount of energy from

the resolved scales.[23] For each filter, three different filter widths have been considered. Fig. 2 sketches the effect of these filter widths on the one-dimensional (streamwise) frequency spectrum, $E(\omega)$,[24] computed for the $Re_\tau = 150$ flow. Since particle dynamics in the viscous sublayer is controlled by flow structures with timescale τ_f around 25 and considering that this timescale corresponds to the circulation time of the turbulence structures in the buffer layer ($5 < z^+ < 30$),[25] we show the energy spectrum at the $z^+ = 25$ location. The cut-off frequencies corresponding to each filter width are indicated as $\omega_{\text{cut-off}}^{\text{CF=2}}$, $\omega_{\text{cut-off}}^{\text{CF=4}}$ and $\omega_{\text{cut-off}}^{\text{CF=8}}$ in increasing order. Also shown (dot-dashed lines) are the estimated response frequencies which characterize each particle set considered in the *a priori* tests, these frequencies being proportional to $1/\tau_p$. Areas filled with patterns below the energy profile represent the relative amount of energy removed by each filter width: larger filter widths prevent particles from being exposed to ever-increasing turbulent frequencies, namely to smaller and smaller flow scales which can modify significantly their local behavior, dispersion and segregation. Inaccurate estimation of these processes due to filtering will bring sub-grid errors into subsequent particle motion.

Fig. 3 shows the particle root mean square (rms) velocity fluctuations obtained in the *a priori* tests with cut-off filter for the $St = 1$, the $St = 5$ and the $St = 25$ particles, respectively. The reference values obtained injecting the particles in the DNS flow velocity fields are also reported. Specifically, the streamwise and wall-normal rms components are shown in Figs. 3(a-c) and Figs. 3(d-f). All profiles were obtained averaging in time (from $t^+ = 450$ to $t^+ = 1200$) and space (over the homogeneous directions). It is apparent that filtering the fluid velocity has a large impact on the turbulent velocity fluctuations. As expected, particle velocity fluctuations are reduced in particular for the larger filter widths corresponding to coarser LES grids. This is consequence of the well known decrease of the flow velocity fluctuations due to filtering as felt by the particles, even if in a different measure depending on their inertia. Note, however, that the effect of filtering is significant also on particles having characteristic response frequencies much lower than those removed by the filters (e.g. the $St = 25$ particles). Finally, for the cut-off filter, underestimation of the particle fluctuations is a pure effect of the elimination of the SGS scales, since no energy is

subtracted from the resolved ones. The results obtained with the top-hat filter (not shown here for brevity) are qualitatively similar, although, for a given filter width, underestimation of the particle fluctuations is, as expected, larger for the top-hat filter than for the cut-off one. The reduction of the wall-normal velocity fluctuations near the wall for the *a priori* LES, shown in Figs. 3(d-f), is worth noting because it corresponds to a reduction of particle turbophoretic drift (namely, particle migration to the wall in turbulent boundary layers) and, in turn, to a reduction of particle accumulation in the near-wall region.[10] This is also shown in Fig. 4 in which the near wall instantaneous particle concentration obtained in *a priori* LES is compared to the DNS one for different filter widths and particle inertia. Concentration profiles shown here are taken at time $t^+ = 1200$: as mentioned, the particle tracking in *a priori* LES was not carried out long enough to reach a statistically-steady particle concentration at the wall. However, we checked many different time instants and, although the concentration values change, the trend is always the same as that shown in Fig. 4. It appears that, consistently with the results of Kuerten and Vreman,[10] filtering leads to a significant underestimation of the wall particle concentration, for all filter types and widths and for all particle sets considered in this study.

Finally, in Fig. 5 the particle segregation parameter, Σ_p, is plotted versus the particle Stokes number in two different regions of the channel: the channel centerline, where Σ_p has been computed in a fluid slab 10 wall unit thick centered at $z^+ = 150$, and in the near-wall region, where Σ_p has been computed in the viscous sublayer ($0 \leq z^+ \leq 5$). The segregation parameter (or maximum deviation from randomness)[26] is calculated as $(\sigma - \sigma_{Poisson})/m$, where σ and $\sigma_{Poisson}$ represent respectively the standard deviations for the particle number density distribution and the Poisson distribution. The particle number density distribution is computed on a grid containing N_{cell} cells of volume Ω_{cell} covering the entire computational domain. The parameter m is the mean number of particles in one cell for a random uniform particle distribution.[26,27] The drawback of this method is the dependence of Σ_p on the cell size. To avoid this problem, we computed the particle number density distribution for several values of Ω_{cell} and we kept only the largest value of Σ_p.[14] First, as found in previous studies,[25] for this shear Reynolds number a peak of Σ_p occurs for $St \simeq 25$ and preferential

concentration falls off on either side of this *optimum* value. As shown for instance in Fig. 4, $St = 25$ particles are thus the most responsive to the near-wall turbulent structures. When an explicit filter is applied, particle segregation is underpredicted severely in all considered cases, especially near the wall. Note that this underestimation is significant also for the smallest filter width, for which the reduction of particle fluctuations was relatively small (see Fig. 3).

3.2. Particle distribution in *a posteriori* LES at Re_τ=150

In this Section, we will discuss the behavior of particles dispersed in LES flow fields. Two different LES grids have been used, as shown in Table I. In these *a posteriori* tests, different sources of errors are present in addition to the filtering effects discussed in Sec. 3.1, viz. the errors due to *(i)* the SGS modeling for the fluid phase, *(ii)* the numerical discretization of the fluid governing equations and *(iii)* the interpolation in the Lagrangian particle tracking. For the used pseudo-spectral discretization the numerical error should plausibly be negligible. As for interpolation, a 6^{th}-order interpolation scheme is used. Although we did not carry out a sensitivity study, the analysis in Kuerten and Vreman[10] indicates that the interpolation error should remain small, even if it may introduce an additional smoothing. Thus, we believe that the main source of difference with the *a priori* tests is represented by the SGS model closing the governing equations for the fluid phase. As in the *a priori* tests, no closure model is used in the equations of particle motion.

In order to asses the quality of the LES for the fluid part, Fig. 6 compares the streamwise and wall-normal rms of the fluid velocity components obtained in LES to the reference DNS values. For the more resolved LES, a good agreement with DNS is obtained and, hence, this can be considered as a *well-resolved* LES for the fluid phase. Conversely, in the coarser LES significant errors are found in the prediction of the fluid-phase velocity fluctuations and, thus, errors in the Lagrangian particle tracking are anticipated. The effect of the SGS modeling error is clearly visible if the values obtained for the coarser grid are compared with those of the *a-priori* tests in Fig. 3 for a corresponding coarsening factor (CF=4).

Indeed, in the *a posteriori* LES, the introduction of the SGS model tends to counteract the decrease of the fluid velocity fluctuations due to filtering; in the coarser case this leads to an overestimation of the rms of the streamwise and wall-normal velocity components. This overestimation is a rather well-known behavior of coarse LES, especially for the rms of the streamwise component. Nonetheless, it is worth remarking that in actual LES the fluid velocity fields in which the particles are dispersed are not always characterized by a lack of fluctuations, as it happens in the idealized context of *a priori* tests. As previously mentioned, the dynamic eddy-viscosity model[15] was used to close the LES equations for the fluid phase. We also carried out LES simulations with the Smagorinsky model, but, as expected, the results were generally less accurate than those obtained with the dynamic SGS model for a fixed resolution: hence they are not shown or discussed here for sake of brevity.

In Fig. 7 the streamwise and wall-normal rms of the different particle sets obtained in LES are compared with the reference DNS data. A good agreement with DNS is obtained in the more resolved LES for all the considered particle inertia, while for the coarser simulation significant discrepancies are found. Note that in the coarse case, the rms of the wall-normal velocity component are overestimated for all the considered particle sets, as previously observed also for the fluid phase. In spite of the differences in the fluid and particle velocity fluctuations observed in *a priori* and *a posteriori* tests, the underestimation of particle concentration at the wall, already observed in the *a priori* tests (see Sec. 3.1), is also found in *a posteriori* LES, for all considered resolutions and particle sets. This is shown, for instance, by the instantaneous particle concentration profiles of Fig. 8. The same is for the underprediction of the particle preferential concentration (see Fig. 9). It is worth nothing that the errors on the quantitative prediction of both particle segregation and near-wall accumulation are large also for the well-resolved LES, in which the level of fluid and particle velocity fluctuations is rather well predicted. This indicates that, in order to obtain acceptable predictions for near-wall accumulation and particle segregation, the reintroduction of the correct level of velocity fluctuations is not the only issue to devise a closure model for the particle equations. Finally, in the *a posteriori* LES the segregation

parameter, Σ_p, was also computed for $St = 125$ particles (see Fig. 9). For this set of particles, the values obtained in both LES simulations are higher than those computed in DNS. In their *a priori* tests for homogeneous and isotropic turbulence, Fede and Simonin[4] found that for particles having lower inertia than a given threshold value the effect of filtering was to decrease the segregation parameter, while for particles of larger inertia the segregation was conversely increased. From our results, this scenario seems to hold also in *a posteriori* LES and in near wall turbulence.

3.3. Influence of the Reynolds number on particle distribution

A priori and *a posteriori* simulations have emphasized that the importance of SGS velocity fluctuations in predicting the properties of particle dispersion depends both on particle inertia, parametrized quantitatively by the particle Stokes number, and on the spatial resolution of the Eulerian grid. The results shown in previous sections, however, are relative to a turbulent channel flow at $Re_\tau = 150$, a rather small value compared to those typical of LES applications. If higher values of Re_τ are to be considered, then Reynolds number effects on particle dispersion may become significant because the characteristic length and time scales of the particle change with respect to those of the fluid when the flow dynamics change: in particular, the higher the Reynolds number the smaller the particle response time for a given value of the Stokes number (see discussion in Sec. 2.4). This point can be further elucidated considering Fig. 10, where the frequency spectrum, $E(\omega)$ computed for the Re^l_τ-DNS (already shown in Fig. 2) is compared with the frequency spectrum computed for the Re^h_τ-DNS. The spectrum is computed at a wall-normal distance $z^+ = 25$ consistently with the reasons discussed in Fig. 2. As done in that figure, the characteristic response frequencies of the particles are also shown. It is apparent that, in the Re^h_τ-flow *(i)* the turbulent kinetic energy budget is associated to a wider range of frequencies, namely to smaller flow timescales with which the particles may interact, and *(ii)* a given value of frequency corresponds to higher values of the turbulent kinetic energy. In this case, applying cut-off frequencies like those shown in Fig. 2 will remove a wider spectrum of flow scales and a larger

amount of turbulent kinetic energy from the flow with respect to the lower Reynolds number flow, thus magnifying the error-behavior of the model in predicting particle segregation and wall accumulation.

In principle, these observations should lead to the conclusion that SGS models must incorporate a dependency on the flow Reynolds number. In fact, the need to include Reynolds number effects should be assessed carefully being based on the knowledge of how particle preferential concentration scales with Re_τ. Numerical investigations on the Reynolds number scaling properties of the preferential concentration of heavy particles have been performed in a synthetic turbulent advecting field by Olla[28] and in homogeneous isotropic turbulence by Collins and Keswani.[29] Here, we investigate on the same effect in turbulent channel flow.

To introduce our scaling argument, let us rewrite Eq. (9) for the case of constant particle response time (namely $\tau_p^h = \tau_p^l$). We have:

$$\frac{St^h}{St^l} = \frac{\tau_f^l}{\tau_f^h} = \left(\frac{u_\tau^h}{u_\tau^l}\right)^2 = \left(\frac{Re_\tau^h}{Re_\tau^l}\right)^2 = 4 \ . \tag{10}$$

From Eq. (10) we can conclude the following: if the shear velocity is the proper scaling parameter to quantify the Reynolds number effect on particle preferential concentration then the statistical description of the $St^h = 4$ particles behavior in the Re_τ^h-flow is expected to resemble that of the $St^l = 1$ particles behavior in the Re_τ^l-flow. Similarly, scaling effects are expected to couple the $St^h = 20$ particles to the $St^l = 5$ particles and the $St^h = 100$ particles to the $St^l = 25$ particles, respectively. We thus expect that, for instance, the particle velocity fluctuations should be proportional to the fluid velocity fluctuations within the range of Reynolds number considered in this study, provided that the Reynolds number effect on preferential concentration is scaled properly.

Figure 11 compares *vis-à-vis* the ratios between the particle and the fluid velocity rms components, $v'_{i,rms}/u'_{i,rms}$, normalized to wall variables using the shear velocity as the scaling parameter. The non-dimensional distance from the wall is indicated as z^+/H^+ where $0 \leq z^+ \leq H^+$, H^+ being equal to either Re_τ^l or Re_τ^h. In each panel of Fig. 11, thick lines are used for the Re_τ^l-DNS whereas open symbols refer to the Re_τ^h-DNS. For ease of reading,

$v'_{i,rms}/u'_{i,rms}$ profiles for the streamwise and wall-normal rms components are shifted by a factor of 0.4, up and down respectively. These statistics have been computed averaging over a time window corresponding to the last 720 wall time units of the simulations under statistically-developing conditions for the particle concentration. Rms ratios have been computed for all particle sets, yet comparison is made only between the particle Stokes numbers matching the two different Reynolds numbers according to Eq. (10): namely $St^l = 1$ and $St^h = 4$ (Fig. 11a), $St^l = 5$ and $St^h = 20$ (Fig. 11b), $St^l = 25$ and $St^h = 100$ (Fig. 11c). It is apparent that the profiles, though a bit ragged, overlap quite well even in the near-wall region, where discrepancies (possibly due to the extension of the averaging time window) are limited to very thin slabs inside the viscous sublayer, thus supporting the validity of the adopted scaling.

In Fig. 12 particle segregation in the center of the channel (Fig. 12a) and in the near-wall region (Fig. 12b) is quantified by the segregation parameter Σ_p for the two DNS simulations. Black symbols represent the values of Σ_p for the five sets of particles considered in the Re^l_τ-DNS, whereas open symbols are used for the six sets of particles considered in the Re^h_τ-DNS. Two observations can be made: first, lower segregation occurs at higher Reynolds number for a given value of the particle Stokes number; second, the degree of segregation is nearly same for particle Stokes numbers and shear Reynolds numbers matching the condition given in Eq. (10), as indicated by the dot-dashed lines with arrows. This is particularly true in the near-wall region.

These results seem to indicate that particle preferential concentration scales proportionally to the flow Reynolds number and that the particle Stokes number, defined as particle timescale normalized to wall variables (the shear fluid velocity being the scaling parameter) may be used to characterize the coupling between particles and fluid in the regime where particles preferentially concentrate. These effects appear to be consistent with other observations, most of which refer to the classical Kolmogorov scaling argument[29,30] that predict statistical saturation at higher Reynolds numbers than those considered here.

4. CONCLUSIONS AND FUTURE DEVELOPMENTS

In this paper, the problem of assessing an accurate Eulerian-Lagrangian modeling of heavy particle dispersion in Large Eddy Simulation is addressed. This problem is investigated in a systematic way by performing DNS, *a priori* and *a posteriori* LES coupled with Lagrangian particle tracking of fully developed channel flow, in which different values of the flow Reynolds number and of the particle response time have been considered. The accuracy in the prediction of the particle velocity statistics, near wall accumulation and preferential segregation are assessed through *vis-à-vis* comparison against DNS data.

Consistently with the results of Kuerten and Vreman,[10] the effect of pure filtering in *a priori* tests is to decrease the fluid velocity fluctuations and, in turn, the particle velocity fluctuations, although by different amounts according to particle inertia. This leads to a severe underestimation of particle accumulation at the wall. Extending the analysis to particle segregation, quantified by a macroscopic indicator, we found that filtering leads to a significant underestimation of particle preferential concentration. In conclusion, it appears that a closure model is needed for the particle equations.[8–10,13] In *a posteriori* LES simulations, we have found that the SGS dynamic model, exploited to close the problem for the fluid phase, is able to reintroduce a correct level of fluid velocity fluctuations when a rather fine grid (two times the DNS grid spacing in each direction) is used; the particle velocity fluctuations are also in good agreement with those obtained in DNS. Conversely, significant discrepancies are observed with respect to the DNS reference values when a coarser resolution (typical of LES applications) is used. We observe that the velocity fluctuations of both phases are overestimated, in contrast with the *a priori* tests. Despite these differences, particle wall accumulation and local segregation are always severely underestimated. This indicates that the reintroduction of the correct level of fluid and particle velocity fluctuations is not the only issue for accurate SGS closure models for the particle equations, which apparently is not enough to have an accurate prediction of near-wall accumulation and local particle segregation. It may be argued that, since these phenomena are governed by complex interactions between the particles and the flow structures, the reitroduction of the correct

amount of higher order moments of the velocity fluctuations for both phases is probably the key point to develop these models. This could be achieved, for instance, using non-Gaussian stochastic Lagrangian models based on Langevin-type equations.[31]

Another important feature of SGS models for particles is that they are required to account for possible flow Reynolds number effects on particle accumulation and segregation. Albeit the Reynolds number range limitations of this study, we have shown that scaling of statistics seems to persist for the Reynolds numbers considered ($Re_\tau = 150$ and 300) and therefore it is possible to parametrize Reynolds number effects simply by imposing a quadratic dependence of the particle Stokes number, defined as the ratio of the particle response time to the viscous timescale of the flow, on the shear Reynolds number. Finally, we are aware that the results shown here only cover the lower range of Reynolds numbers typical of LES applications: Hence, one future development (currently under way) of this work will be to investigate on the Reynolds number scaling properties of particle segregation through DNS/LES of turbulent channel flow at $Re_\tau = 600$.

ACKNOWLEDGMENTS

The authors wish to thank A. Mannucci, L. Rigaux and L. Osmar for their help in performing some of the simulations. Support from PRIN (under Grant 2006098584_004) and from HPC Europa Transnational Access Program (under Grants 466 and 708) are gratefully acknowledged.

REFERENCES

[1] L. P. Wang and M. R. Maxey, "Settling velocity and concentration distribution of heavy particles in homogeneous isotropic turbulence," J. Fluid Mech. **256**, 27 (1993).

[2] C. Marchioli and A. Soldati, "Mechanisms for particle transfer and segregation in turbulent boundary layer," J. Fluid Mech. **468**, 283 (2002).

[3] J. Bec, L. Biferale, M. Cencini, A. Lanotte, S. Musacchio, F. Toschi, "Heavy particle concentration in turbulence at dissipative and inertial scales," Phys. Rev. Lett. **98**, 084502 (2007).

[4] P. Fede and O. Simonin, "Numerical study of the subgrid fluid turbulence effects on the statistics of heavy colliding particles," Phys. Fluids **18**, 045103 (2006).

[5] A. Soldati, "Particles turbulence interactions in boundary layers," Z. Angew. Math. Mech. **85**, 683 (2005).

[6] C. Marchioli, A. Giusti, M. V. Salvetti and A. Soldati, "Direct numerical simulation of particle wall transfer and deposition in upward turbulent pipe flow," Int. J. Multiphase Flow **29**, 1017 (2003).

[7] W. S. J. Uijttewaal and R. W. A. Oliemans, "Particle dispersion and deposition in direct numerical and large eddy simulations of vertical pipe flows," Phys. Fluids **8**, 2590 (1996).

[8] Q. Wang and K. D. Squires, "Large eddy simulation of particle deposition in a vertical turbulent channel flow," Int. J. Multiphase Flow **22**, 667 (1996).

[9] J. G. M. Kuerten, "Subgrid modeling in particle-laden channel flow," Phys. Fluids **18**, 025108 (2006).

[10] J. G. M. Kuerten and A. W. Vreman, "Can turbophoresis be predicted by large-eddy simulation?," Phys. Fluids **17**, 011701 (2005).

[11] V. Armenio, U. Piomelli and V. Fiorotto, "Effect of the subgrid scales on particle motion," Phys. Fluids **11**, 3030 (1999).

[12] M. W. Reeks, "The transport of discrete particles in inhomogeneous turbulence," J. Aerosol Sci. **14**, 729 (1983).

[13] B. Shotorban and F. Mashayek, "Modeling subgrid-scale effetcs on particles by approximate deconvolution," Phys. Fluids **17**, 081701 (2005).

[14] P. Février, O. Simonin and K. D. Squires, "Partitioning of particle velocities in gas-solid turbulent flows into a continuous field and a spatially-uncorrelated random distribution: theoretical formalism and numerical study," J. Fluid Mech. **528**, 1 (2005).

[15] M. Germano, U. Piomelli, P. Moin and W. H. Cabot, "A dynamic subgrid-scale eddy viscosity model," Phys. Fluids **3**, 1760 (1991).

[16] S. E. Elghobashi and G. C. Truesdell, "Direct simulation of particle dispersion in a decaying isotropic turbulence," J. Fluid Mech. **242**, 655 (1992).

[17] C. Crowe, M. Sommerfeld and T. Tsuji, *Multiphase flows with droplets and particles* CRC Press, New York (1998).

[18] Y. Pan and S. Banerjee, "Numerical simulation of particle interactions with wall turbulence," Phys. Fluids **17**, 2733 (1996).

[19] In the present flow configuration, the non-dimensional Kolmogorov length scale, η_K^+, varies along the wall-normal direction from a minimum value $\eta_K^+ = 1.6$ at the wall to a maximum value $\eta_K^+ = 3.6$ at the centerline. The grid resolution in the wall-normal direction is such that the first collocation point is at $z^+ = 0.05$ from the wall, while in the center of the channel $\Delta z^+ = 3.7$

[20] S. Pope, "Ten questions concerning the large-eddy simulation of turbulent flows," New J. Phys. **6**, 1 (2004).

[21] C. Marchioli, A. Soldati, J. G. M. Kuerten, B. Arcen, A. Tanière, G. Goldensoph, K. D. Squires, M. F. Cargnelutti and L. M. Portela, Statistics of particle dispersion in Direct Numerical Simulations of wall-bounded turbulence: results of an international collaborative benchmark test," Int. J. Multiphase Flow, Submitted (2007).

[22] C. Marchioli, M. Picciotto and A. Soldati, "Particle dispersion and wall-dependent fluid scales in turbulent bounded flow: implications for local equilibrium models," J. Turbulence **27**, 1 (2006).

[23] P. Sagaut, *Large Eddy Simulation for incompressible flows* Springer-Verlag, Berlin (2001).

[24] Pope, S. *Turbulent flows* Cambridge University Press, Cambridge (2000).

[25] M. Picciotto, C. Marchioli and A. Soldati, "Characterization of near-wall accumulation regions for inertial particles in turbulent boundary layers," Phys. Fluids **17**, 098101 (2005).

[26] D. W. Rouson and J. K. Eaton, "On the preferential concentration of solid particles in turbulent channel flow," J. Fluid Mech. **428**, 149 (2001).

[27] Here random is defined as the situation in which any given particle is equally likely to appear in any given cell so that one can show that the particle number distribution approaches a Poisson distribution (Ref.[26]).

[28] P. Olla, "Transport properties of heavy particles in high Reynolds number turbulence," Phys. Fluids **14**, 4266 (2002).

[29] L. R. Collins and A. Keswani, "Reynolds number scaling of particle clustering in turbulent aerosols," New J. Phys. **6**, 1 (2004).

[30] P. K. Yeung, S. B. Pope and B. L. Sawford, "Reynolds number dependence of Lagrangian statistics in large numerical simulations of isotropic turbulence," J. Turbulence **7**, 1 (2006).

[31] I. Iliopoulos and T. J. Hanratty, "A non-Gaussian stochastic model to describe passive tracer dispersion and its comparison to a direct numerical simulation," Phys. Fluids **16**, 3006 (2004).

TABLES

Re_τ	DNS	*a-priori* LES	*a-posteriori* LES
		$64 \times 64 \times 129$ (CF=2)	$64 \times 64 \times 65$
150 ($=Re^l_\tau$)	$128 \times 128 \times 129$	$32 \times 32 \times 129$ (CF=4)	$32 \times 32 \times 65$
		$16 \times 16 \times 129$ (CF=8)	—
300 ($=Re^h_\tau$)	$256 \times 256 \times 257$	—	—

TABLE I. Summary of the simulations.

$St^l = St\|_{Re^l_\tau}$	τ^l_p (s)	d^+_p	d_p (μm)	$V^+_s = g^+ \cdot St$	$Re^+_p = V^+_s \cdot d^+_p/\nu^+$
0.2	$0.227 \cdot 10^{-3}$	0.068	9.1	0.0188	0.00128
1	$1.133 \cdot 10^{-3}$	0.153	20.4	0.0943	0.01443
5	$5.660 \cdot 10^{-3}$	0.342	45.6	0.4717	0.16132
25	$28.32 \cdot 10^{-3}$	0.765	102.0	2.3584	1.80418
125	$1.415 \cdot 10^{-1}$	1.71	228	11.792	20.1643

TABLE II. Particle parameters for the Re^l_τ simulations.

$St^h = St\|_{Re^h_\tau}$	τ^h_p (s)	d^+_p	d_p (μm)	$V^+_s = g^+ \cdot St$	$Re^+_p = V^+_s \cdot d^+_p/\nu^+$
1	$0.283 \cdot 10^{-3}$	0.153	10.2	0.0118	0.00275
4	$1.132 \cdot 10^{-3}$	0.306	20.4	0.0472	0.01444
5	$1.415 \cdot 10^{-3}$	0.342	22.8	0.0590	0.02018
20	$5.660 \cdot 10^{-3}$	0.684	45.6	0.2358	0.16129
25	$7.075 \cdot 10^{-3}$	0.765	51.0	0.2948	0.22552
100	$28.30 \cdot 10^{-3}$	1.530	102.0	1.1792	1.80418

TABLE III. Particle parameters for the Re^h_τ simulations.

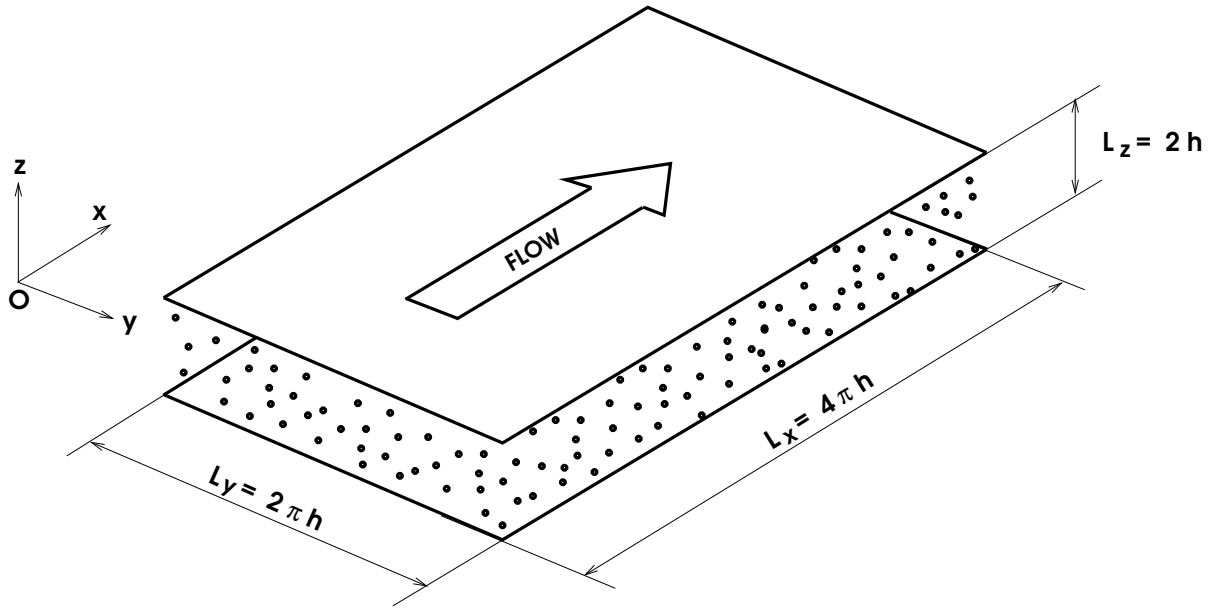

FIG. 1. Particle-laden turbulent gas flow in a flat channel: computational domain.

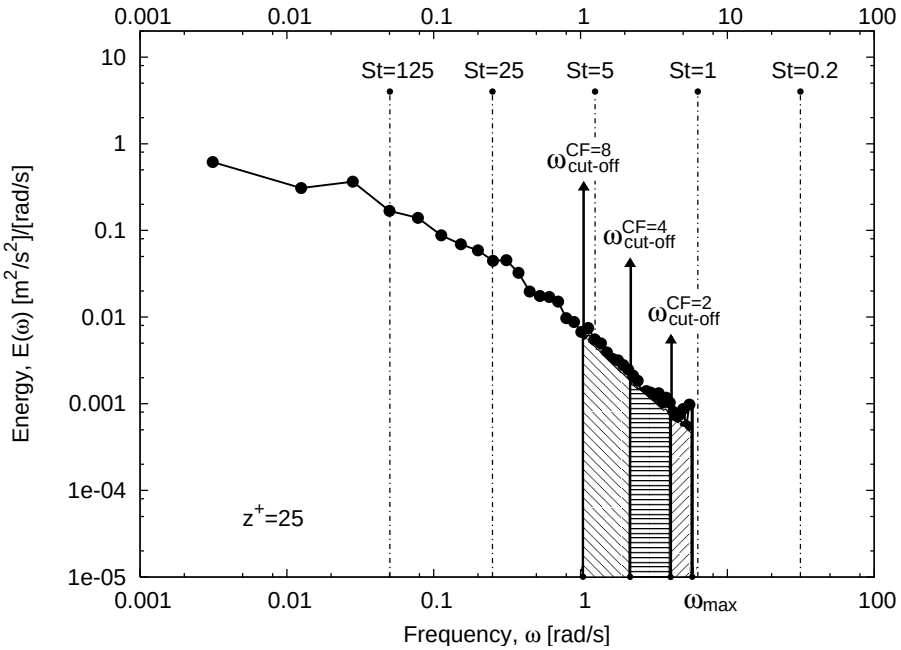

FIG. 2. One-dimensional (streamwise) frequency spectrum for turbulent channel flow at $Re_\tau = 150$, computed at $z^+ = 25$ at $Re_\tau = 150$. The different cut-off frequencies, used to perform the *a-priori* tests, are indicated as $\omega_{\text{cut-off}}^{\text{CF=2}}$, $\omega_{\text{cut-off}}^{\text{CF=4}}$ and $\omega_{\text{cut-off}}^{\text{CF=8}}$, respectively. Areas filled with patterns below the energy profile represent the relative amount of energy removed by each cut-off.

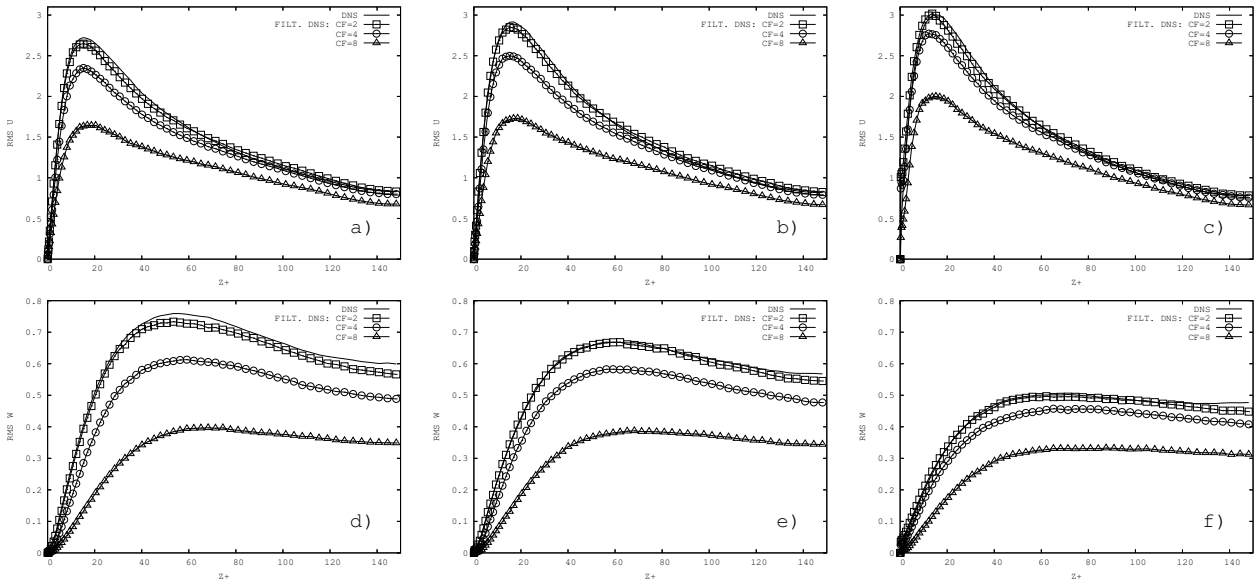

FIG. 3. Particle rms velocity fluctuations for *a priori* simulations (with cut-off filter) without SGS modeling in the particle equation of motion: (a-c) streamwise rms component, (d-f) wall-normal rms component. Left-hand panels: $St = 1$ particles, central panels: $St = 5$ particles, right-hand panels: $St = 25$ particles. CF indicates the LES grid coarsening factor with respect to the DNS grid: CF=2 (□), CF=4 (◯), CF=8 (△).

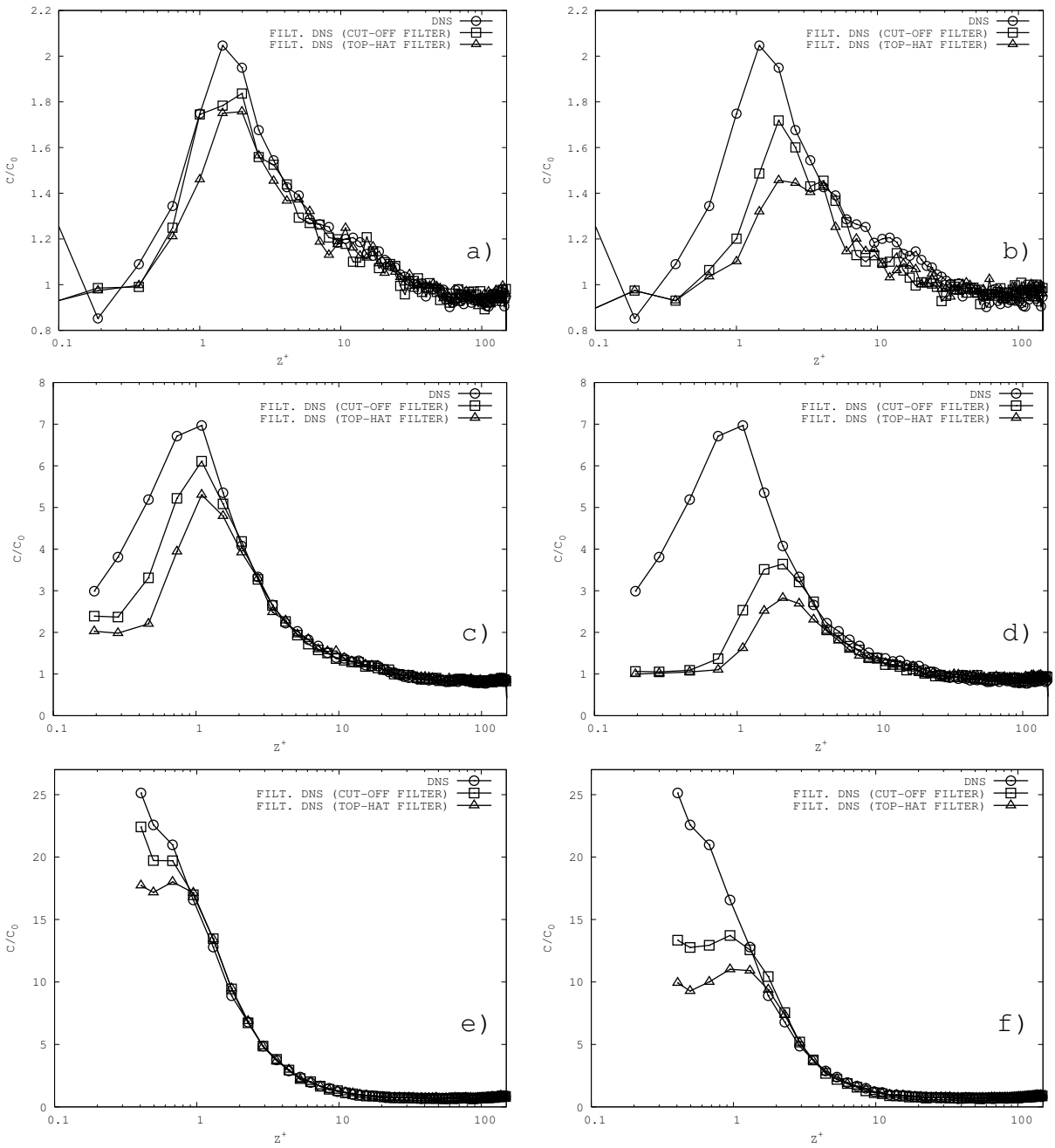

FIG. 4. Particle concentration in *a-priori* tests without SGS modeling in the particle equation of motion: (a-b) $St = 1$ particles, (c-d) $St = 5$ particles, (e-f) $St = 25$ particles. DNS (◯), *a-priori* LES with cut-off filter (□), *a-priori* LES with top-hat filter (△). Left-hand panels: tests on the fine $64 \times 64 \times 65$ grid (CF=2), right-hand panels: tests on the coarse $32 \times 32 \times 65$ grid (CF=4).

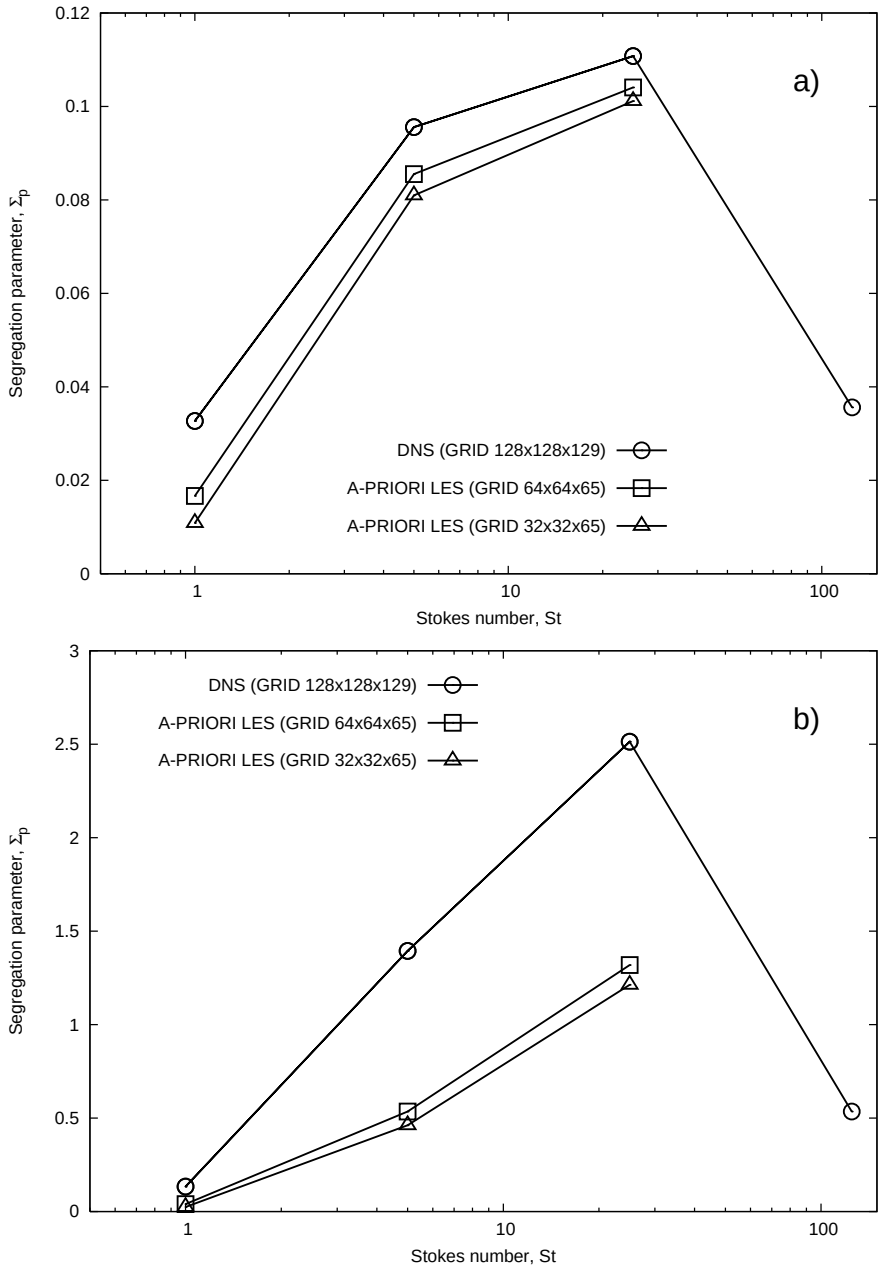

FIG. 5. Particle segregation, Σ_p, versus particle Stokes number, St, in turbulent channel flow: comparison between DNS (◯), *a-priori* LES on the fine $64 \times 64 \times 65$ grid (□) and *a-priori* LES on the coarse $32 \times 32 \times 65$ grid (△). *A-priori* results are relative to the cut-off filter. Panels: (a) channel centerline ($145 \leq z^+ \leq 150$), (b) near-wall region ($0 \leq z^+ \leq 5$).

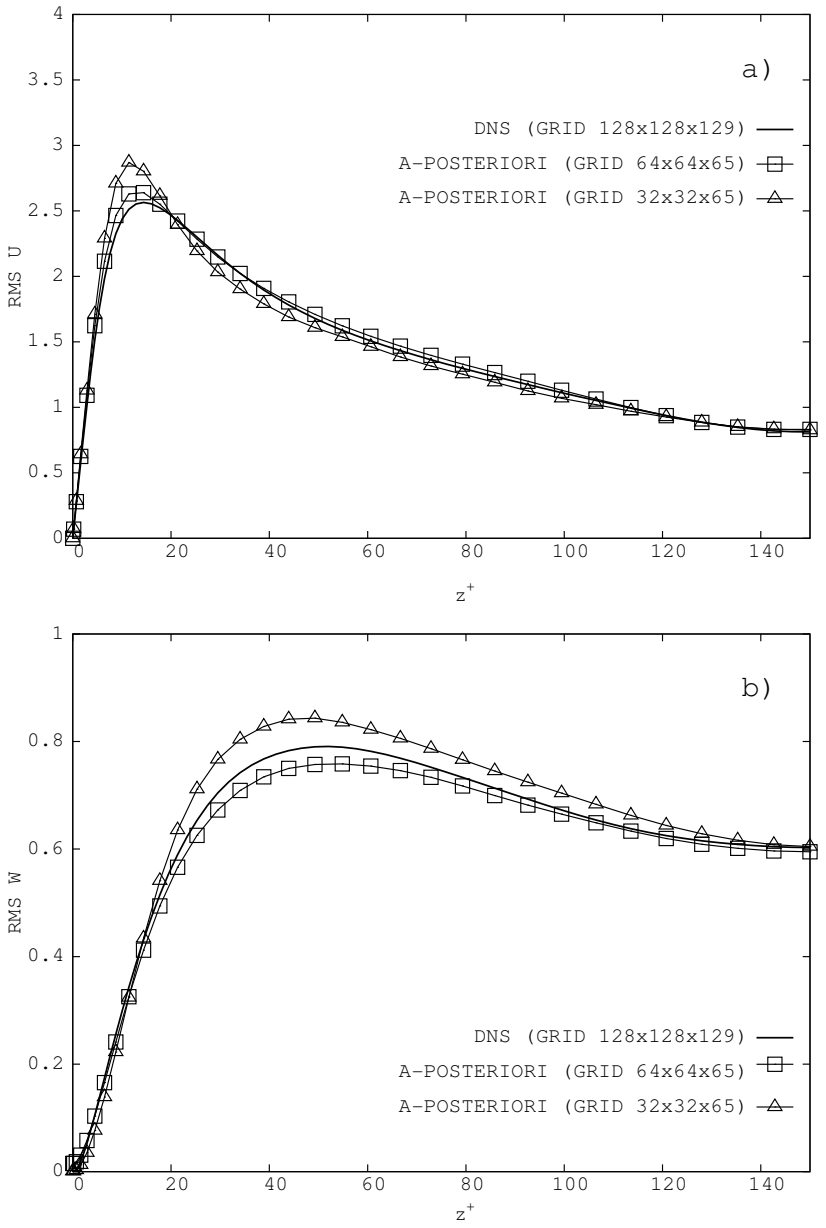

FIG. 6. Fluid rms velocity fluctuations: comparison between DNS (solid line), *a-posteriori* LES on the fine $64 \times 64 \times 65$ grid ($\square$) and *a-posteriori* LES on the coarse $32 \times 32 \times 65$ grid ($\triangle$). Panels: (a) streamwise rms component, (b) wall-normal rms component.

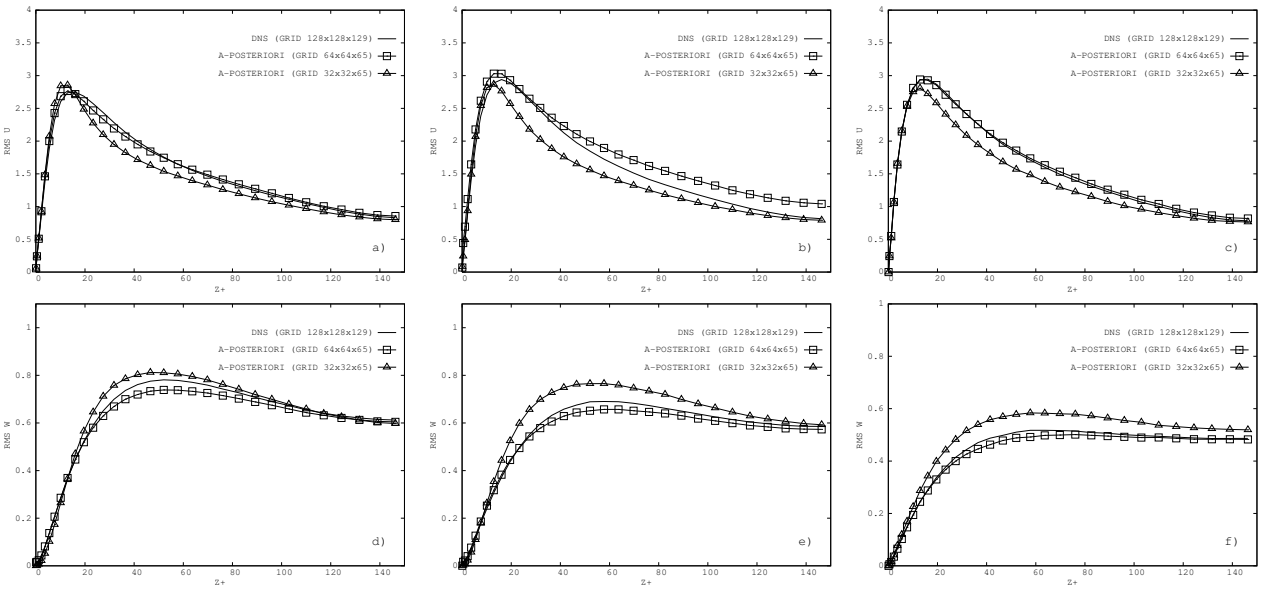

FIG. 7. Particle rms velocity fluctuations: comparison between DNS (solid line), *a-posteriori* LES on the fine $64\times64\times65$ grid ($\square$) and *a-posteriori* LES on the coarse $32\times32\times65$ grid ($\triangle$): (a-c) streamwise rms component, (d-f) wall-normal rms component. Left-hand panels: $St = 1$ particles, central panels: $St = 5$ particles, right-hand panels: $St = 25$ particles.

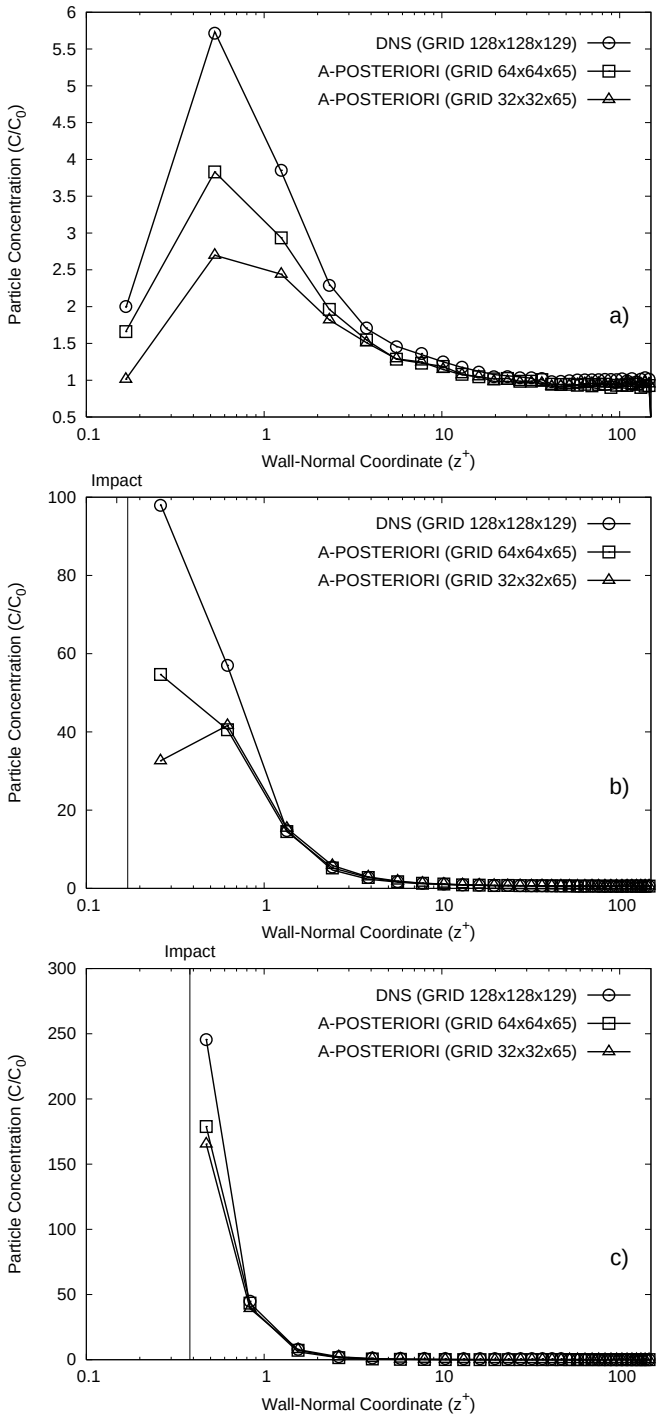

FIG. 8. Particle concentration in *a-posteriori* tests without SGS modeling in the particle equation of motion: comparison between DNS (◯), *a-posteriori* LES on the fine $64 \times 64 \times 65$ grid (□) and *a-posteriori* LES on the coarse $32 \times 32 \times 65$ grid (△). Panels: (a) $St = 1$ particles, (b) $St = 5$ particles, (c) $St = 25$ particles. The vertical solid line in each diagram indicates the position where the particles hit the wall (*Impact*): note that impact for the $St = 1$ particles occurs at $z^+ = 0.034$, outside the z^+-range covered in panel (a).

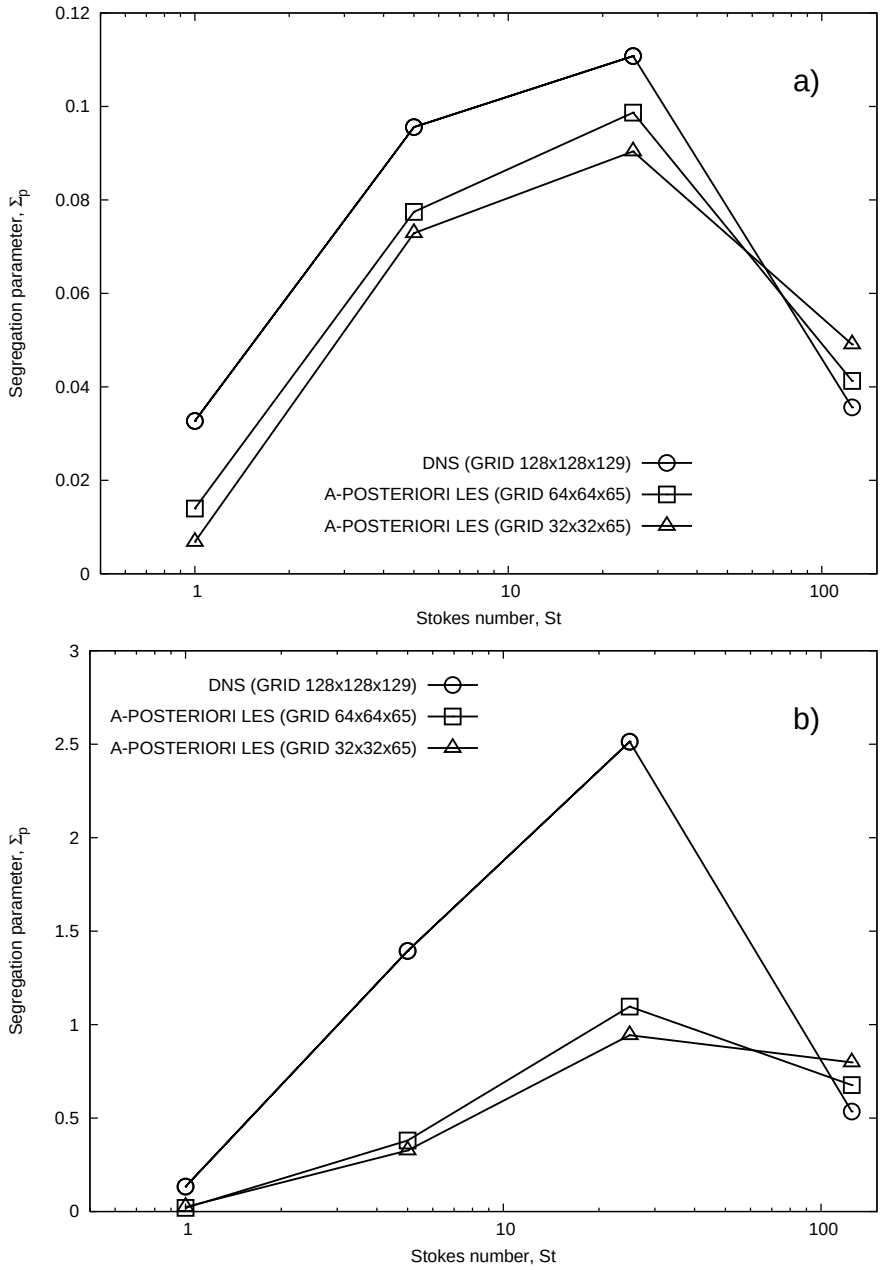

FIG. 9. Particle segregation, Σ_p, versus particle Stokes number, St, in turbulent channel flow: comparison between DNS (◯), *a-posteriori* LES on the fine $64 \times 64 \times 65$ grid (□) and *a-posteriori* LES on the coarse $32 \times 32 \times 65$ grid (△). Panels: (a) channel centerline ($145 \leq z^+ \leq 150$), (b) near-wall region ($0 \leq z^+ \leq 5$).

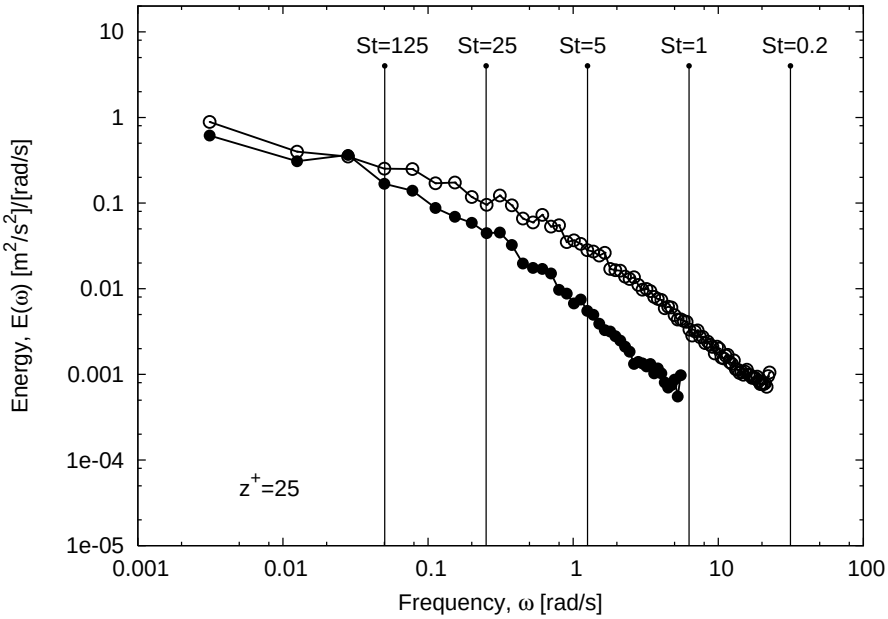

FIG. 10. One-dimensional (streamwise) frequency spectrum for turbulent channel flow computed at $z^+ = 25$ for two different Reynolds numbers: $Re_\tau^l = 150$ (•) and $Re_\tau^h = 300$ (○).

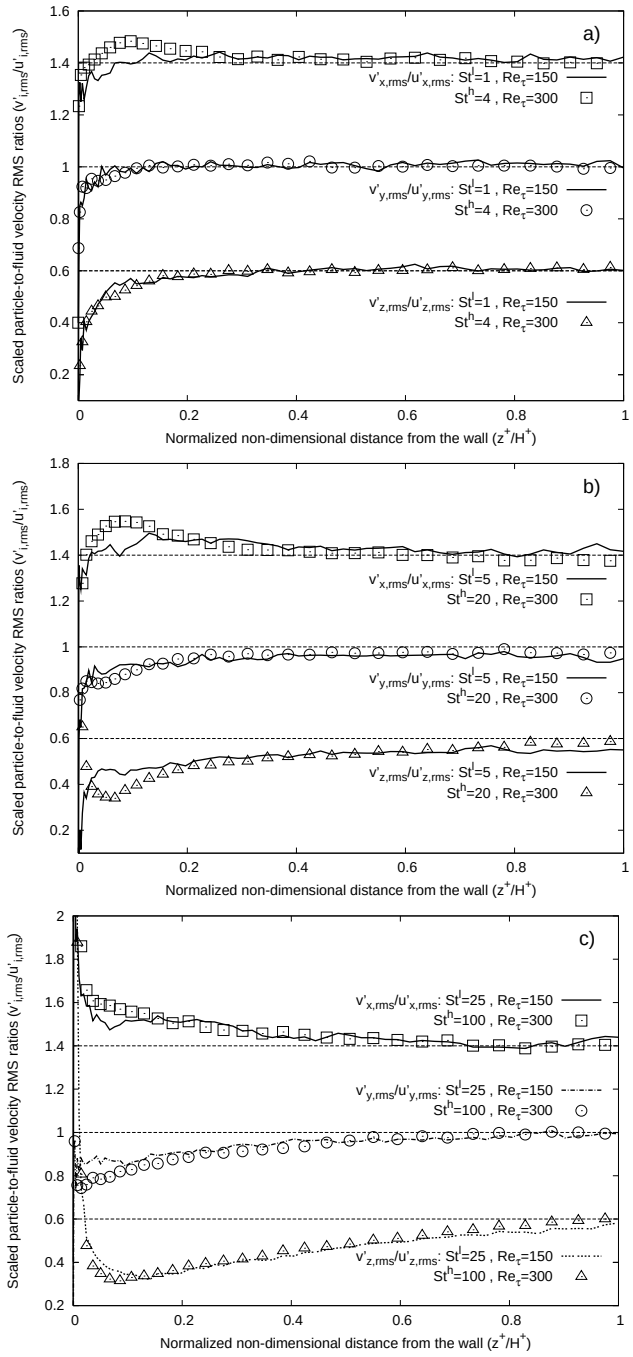

FIG. 11. Scaled particle−to−fluid velocity rms ratios at low Reynolds number, $(v'_{i,rms}/u'_{i,rms})|_{St^l,Re^l_\tau}$, and at high Reynolds number, $(v'_{i,rms}/u'_{i,rms})|_{St^h,Re^h_\tau}$. Panels: (a) $St^l = 1$ versus $St^h = 4$, (b) $St^l = 5$ versus $St^h = 20$, (c) $St^l = 25$ versus $St^h = 100$.

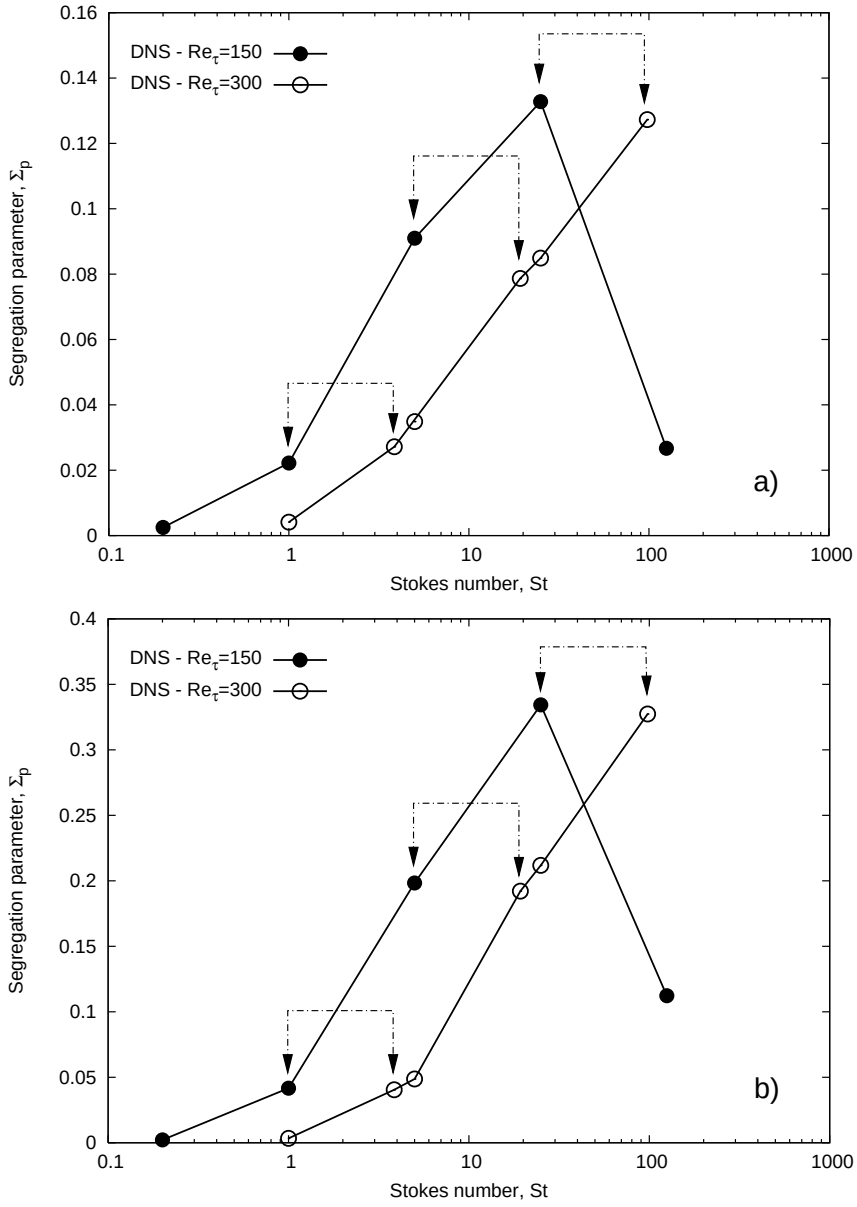

FIG. 12. Particle segregation parameter, Σ_p, versus particle Stokes number, St, in turbulent channel flow at two different Reynolds numbers: $Re_\tau = 150$ (•) and $Re_\tau = 300$ (○). Panels: (a) channel centerline ($145 \leq z^+ \leq 150$), (b) near-wall region ($0 \leq z^+ \leq 5$).